Chapter 8

Mechanochemical Synthesis of Magnetite/Hydroxyapatite Nanocomposites for Hyperthermia

Tomohiro Iwasaki

Additional information is available at the end of the chapter

http://dx.doi.org/10.5772/54344

1. Introduction

Hydroxyapatite ($Ca_{10}(PO_4)_6(OH)_2$, HA), which is a calcium phosphate ceramic, has been widely used as a biomaterial in various applications (e.g., artificial bone and dental root, cosmetic foundation, etc.) because of its high biocompatibility and chemical stability. Moreover, many attempts are being made to give new functions to HA by incorporating effective components into a HA matrix. In particular, magnetite (Fe_3O_4)-incorporated HA (Fe_3O_4/HA) nanocomposites have attracted much attention as a promising material for hyperthermia therapy of malignant bone tumor [1–4]. Recently, Fe_3O_4/HA composites have also been used as adsorbents [5–7] and catalysts [8,9].

Fe_3O_4/HA composites can be synthesized conventionally by mixing HA powder with Fe_3O_4 nanoparticles which are prepared individually [1–3,5–10]. The conventional synthesis methods have disadvantages: reaction time required for completing the formation of HA and Fe_3O_4 is relatively long, subsequent heat treatments for long periods of time are required for aging and crystallization. Thus, the synthesis of Fe_3O_4/HA composites generally consist of multi-step processes. Therefore, a simple method which can provide Fe_3O_4/HA composites rapidly is needed to be developed.

In this chapter, a mechanochemical method for the simple synthesis of Fe_3O_4/HA nanocomposites is presented. In this method, superparamagnetic Fe_3O_4 nanoparticles are first prepared mechanochemically from ferric hydroxide [11], and then the mechanochemical synthesis of HA from dicalcium phosphate dihydrate ($CaHPO_4\ 2H_2O$) and calcium carbonate ($CaCO_3$, calcite) is performed [12–14], followed by the aging for a short period of time. These mechanochemical treatments are sequentially performed in a single horizon-

tal tumbling ball mill at room temperature under wet conditions. The wet mechanochemical process can also contribute to the distribution of Fe_3O_4 nanoparticles in the HA matrix, which can result in a good hyperthermia property. In addition, the use of horizontal tumbling ball mills is reasonable for the synthesis of Fe_3O_4/HA nanocomposites because the device structure is simple, the handling is easy, the energy consumption is relatively low, and the scale-up is easy [15]. The influence of conditions on the formation of Fe_3O_4/HA nanocomposites was investigated and the hyperthermia property was examined. The details are described below.

2. Mechanochemical synthesis of hydroxyapatite nanoparticles

First of all, the synthesis of HA nanoparticles containing no Fe_3O_4 nanoparticles was investigated to optimize the synthesis process of Fe_3O_4/HA nanocomposites. In all the experiments presented in this chapter, the chemicals of analytical grade were used as received without further purification. Typically, 30 mmol of $CaHPO_4\ 2H_2O$ and 20 mmol of $CaCO_3$, corresponding to the stoichiometric molar ratio in the formation reaction of HA expressed by Equation (1) [14], were added to 60 ml of deionized and deoxygenated water.

$$6CaHPO_4 \cdot 2H_2O + 4CaCO_3 \rightarrow Ca_{10}\left(PO_4\right)_6\left(OH\right)_2 + 14H_2O + 4CO_2 \quad (1)$$

The resulting suspension was subjected to a mechanochemical treatment using a horizontal tumbling ball mill, as illustrated in Figure 1. The suspension was placed in a Teflon-lined milling pot with an inner diameter of 90 mm and a capacity of 500 ml. Zirconia balls with a diameter of 3 mm were used as the milling media; the charged volume of the balls (including voids among the balls) was 40% of the pot capacity. The wet milling was performed at room temperature in air atmosphere under atmospheric pressure for a designated period of time. The rotational speed was 140 rpm, corresponding to the ideal critical rotational speed. After milling, the precipitate was isolated from the suspension by centrifugation, washed with acetone, and dried at room temperature in air. As a control experiment without milling, the starting suspension was vigorously stirred at room temperature for 24 h.

The samples obtained under various conditions were characterized according to standard methods. The powder X-ray diffraction (XRD) pattern of samples was obtained by an X-ray diffractometer (RINT-1500, Rigaku; CuKα radiation, 40 kV, 80 mA, 2θ=5°–50°, scanning rate: 1.0°/min). Figure 2 shows the XRD pattern of samples obtained in different milling times. As the milling time increased, the diffractions indicating the presence of $CaHPO_4\ 2H_2O$ and $CaCO_3$ decreased. Simultaneously, the diffractions indicating HA appeared. In particular, a drastic change was observed between 1 h and 3 h. On the contrary, when stirred for 24 h without milling, the XRD pattern (not shown) hardly changed from the beginning, which was almost the same as that before milling as shown in Figure 2a. These results indicate that the milling promoted the solid phase reaction expressed by Equation (1). However, after

http://dx.doi.org/10.5772/54344

milling for 12 h, the XRD pattern was almost the same and the diffraction at 2θ=29.4°, indicating the presence of $CaCO_3$, still remained even in 24 h.

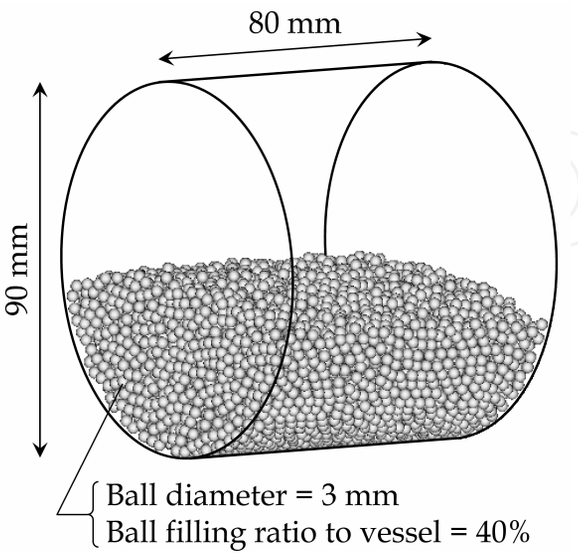

Figure 1. Schematic illustration of horizontal tumbling ball mill used in this work.

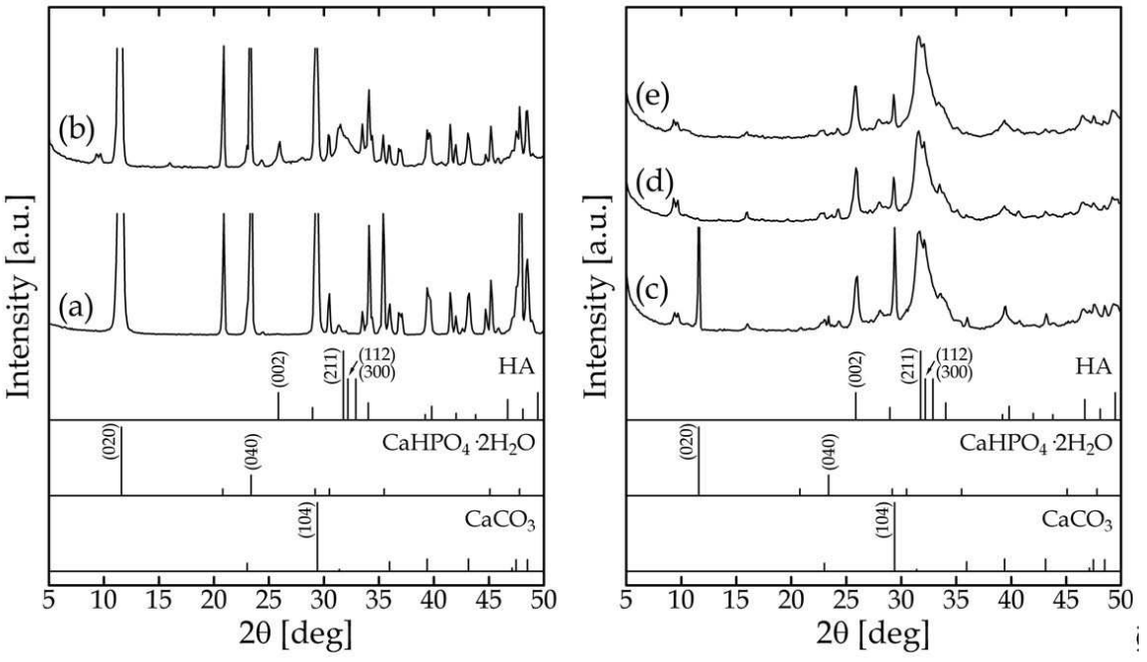

Figure 2. XRD pattern of samples (a) before milling and after milling for (b) 1 h, (c) 3 h, (d) 12 h, and (e) 24 h.

The differential scanning calorimetry (DSC) was performed using a thermal analyzer (SDT2960, TA Instrument) with an argon flow rate of 100 ml/min. The temperature was raised from ambient temperature to 900 °C at a rate of 20°C/min. Figure 3 shows the results

of DSC analysis for the raw materials and the samples. In the sample obtained in 1 h (Figure 3d), the endothermic peaks were clearly observed at around 200°C and 750°C, which resulted from the elimination of water of crystallization in $CaHPO_4$ $2H_2O$ and the thermal decomposition of $CaHPO_4$ $2H_2O$ and $CaCO_3$. Although the peaks relating to $CaHPO_4$ $2H_2O$ disappeared as the milling time, the peak resulted from the thermal decomposition of $CaCO_3$ remained even in 12 h. Accordingly, it was found that the milling was not sufficient to complete the formation reaction of HA.

The morphology of samples was observed by field emission scanning electron microscopy (FE-SEM; JSM-6700F, JEOL). Figure 4 shows typical SEM images of samples. In a milling time of 1 h, coarse particles coated with fine particles of about 100 nm were observed. From the particle size analysis of $CaHPO_4$ $2H_2O$ and $CaCO_3$ by the laser diffraction/scattering method (SALD-7100, Shimadzu), the median sizes were determined to be 16.2 μm for $CaHPO_4$ $2H_2O$ and 2.0 μm for $CaCO_3$. In general, horizontal tumbling ball mills are difficult to produce nanoparticles for short milling times. Therefore, coarse and fine particles could be the raw materials and HA, respectively. As the milling time increased, coarse particles disappeared and the number of HA nanoparticles increased. However, even after 12 h, a little number of coarse particles was found.

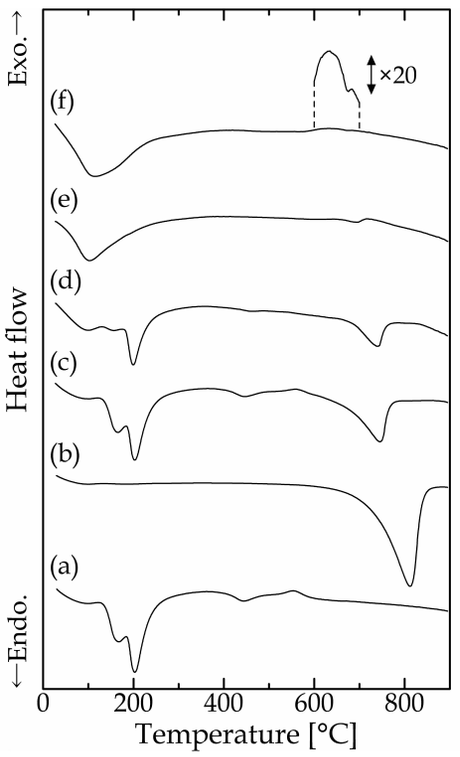

Figure 3. DSC curve of (a) $CaHPO_4$ $2H_2O$, (b) $CaCO_3$, and samples (c) before milling and after milling for (d) 1 h, (e) 3 h, and (f) 12 h.

In order to complete the formation reaction of HA, the heat treatment (aging) was performed after milling. For investigating the effect of heating on the formation of HA, the un-

http://dx.doi.org/10.5772/54344

milled suspension of $CaHPO_4$ $2H_2O$ and $CaCO_3$ was heated under various conditions of temperature and time. Figures 5, 6, and 7 show the XRD patterns of samples obtained without milling after heating at 40, 60, and 80°C, respectively. When the suspension was heated at 40°C, the formation reaction of HA hardly took place. As increasing in the temperature, the reaction was promoted and could complete at 80°C in 8 h. Thus, when without milling, higher heating temperatures and longer heating times are needed for the formation of HA.

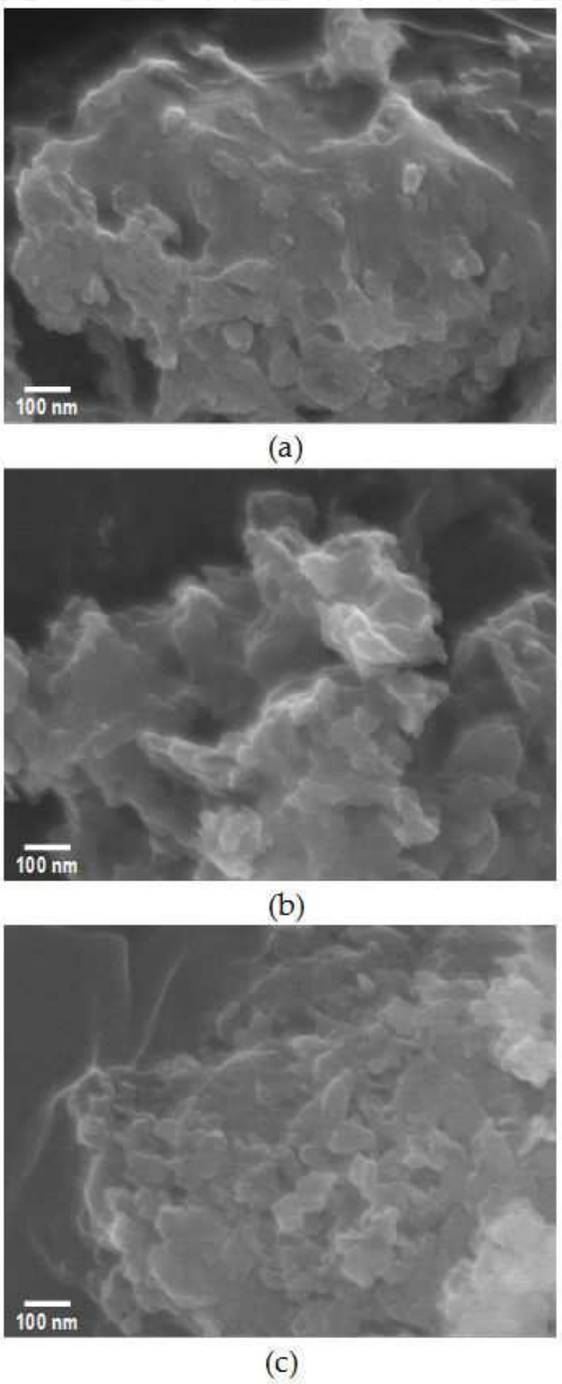

Figure 4. SEM image of samples obtained after milling for (a) 1 h, (b) 3 h, and (c) 12 h.

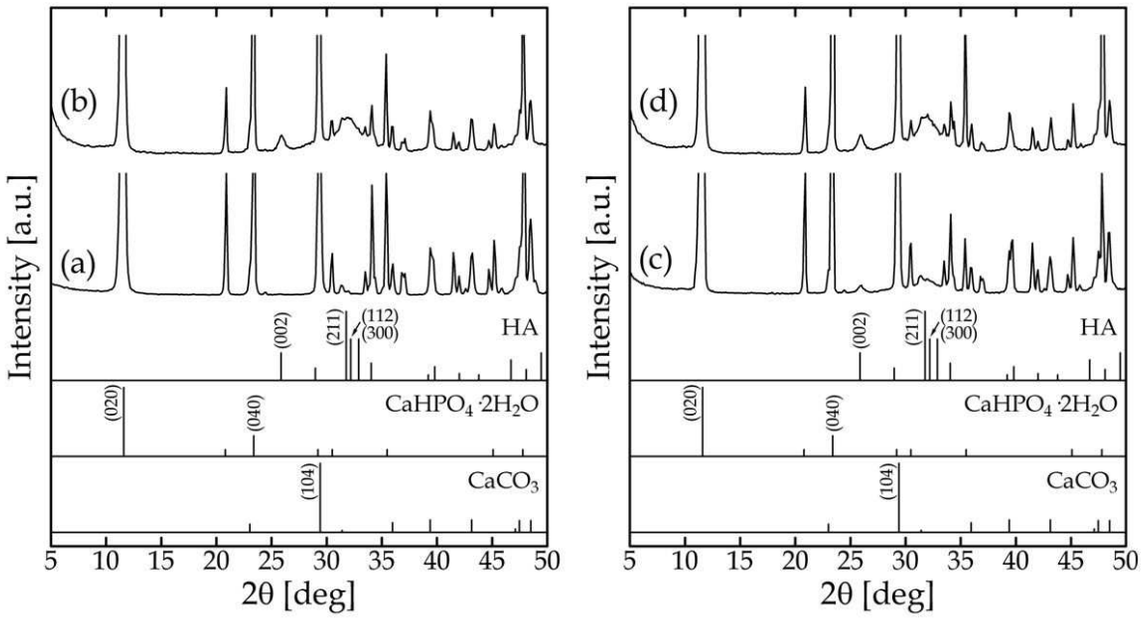

Figure 5. XRD pattern of un-milled samples (a) before heating and after heating at 40°C for (b) 3 h, (c) 5 h, and (d) 8 h.

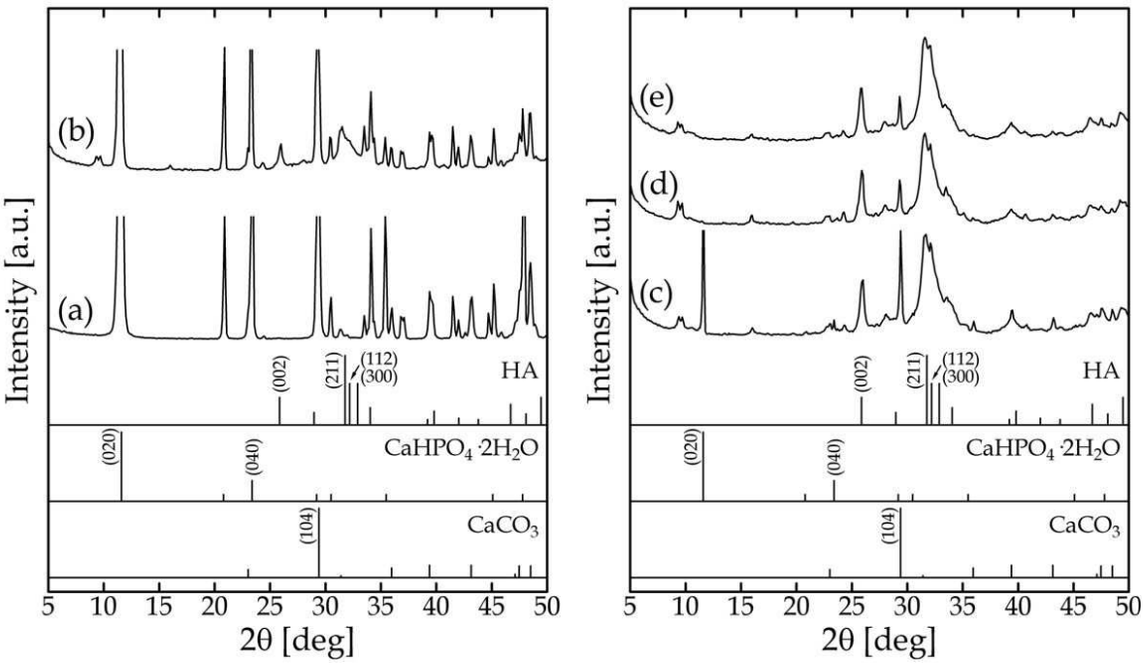

Figure 6. XRD pattern of un-milled samples (a) before heating and after heating at 60°C for (b) 1 h, (c) 3 h, (d) 5 h, and (e) 8 h.

http://dx.doi.org/10.5772/54344

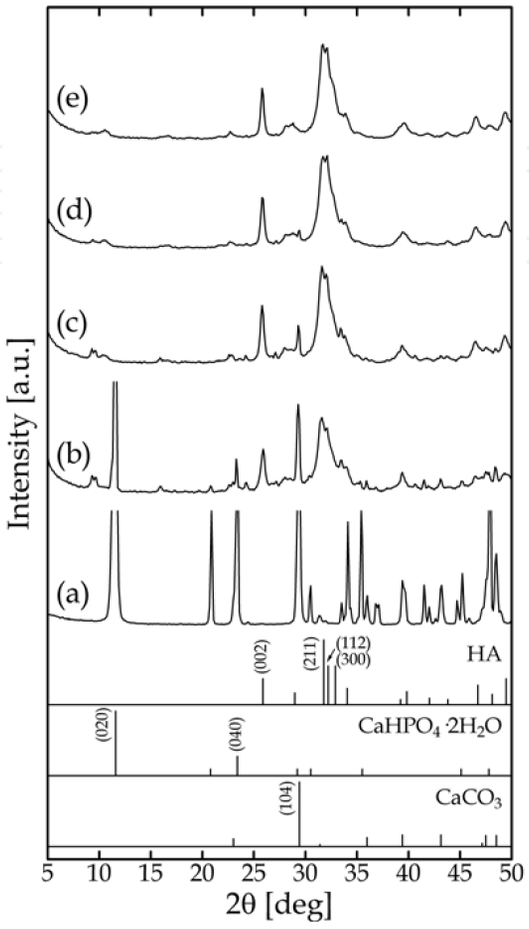

Figure 7. XRD pattern of un-milled samples (a) before heating and after heating at 80°C for (b) 1 h, (c) 3 h, (d) 5 h, and (e) 8 h.

Next, the effect of milling of the suspension before heating on the formation of HA was investigated. Figures 8–14 show the XRD patterns of samples obtained under various conditions of milling time, heating temperature, and heating time. It was found that longer milling times, higher heating temperatures, and longer heating times promoted the formation reaction of HA. In particular, as shown in Figure 10c, when the heating was performed at 80°C, only the milling for 1 h and the following heating for 1 h provided a single phase of HA. The SEM images of samples obtained by milling for different times under constant heating conditions of 80°C and 1 h are shown in Figure 15. When heating at 80°C for 1 h, a typical morphology of HA was observed regardless of the milling time. However, the particle size intended to decrease as the milling time increased. Consequently, the combination of milling and heating of the suspension of $CaHPO_4\ 2H_2O$ and $CaCO_3$ can produce efficiently HA for short periods of time.

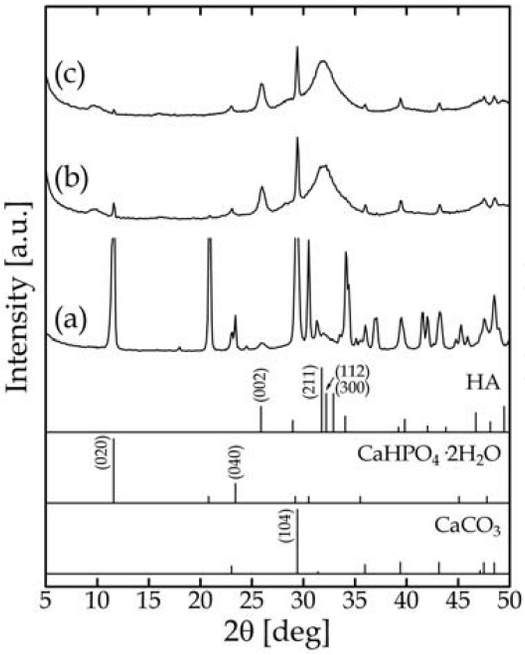

Figure 8. XRD pattern of 1 h-milled samples (a) before heating and after heating at 40°C for (b) 1 h, and (c) 5 h.

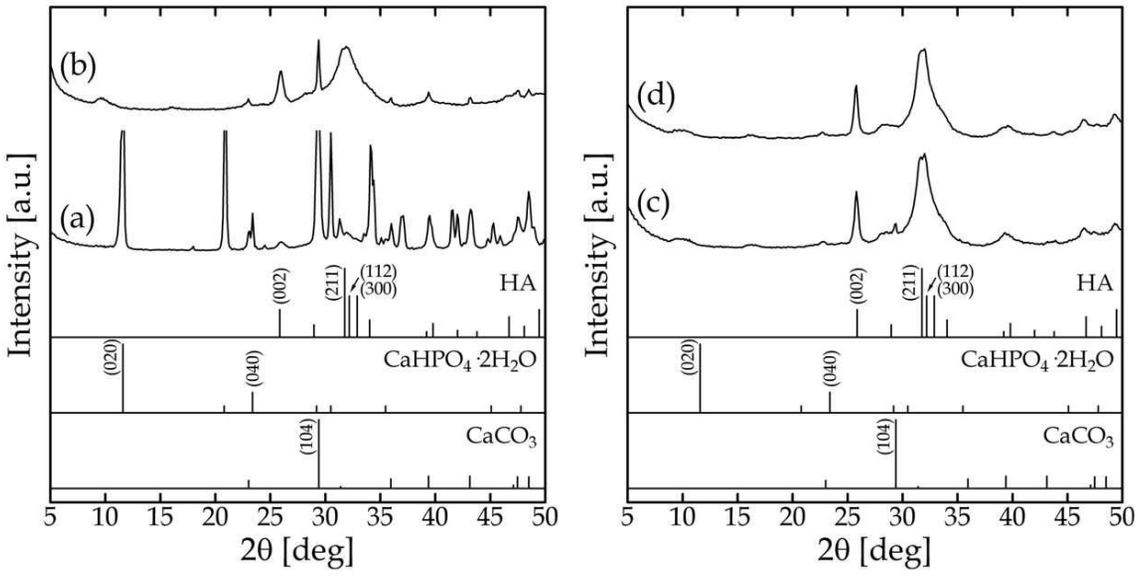

Figure 9. XRD pattern of 1 h-milled samples (a) before heating and after heating at 60°C for (b) 1 h, (c) 3 h, and (d) 5 h.

http://dx.doi.org/10.5772/54344

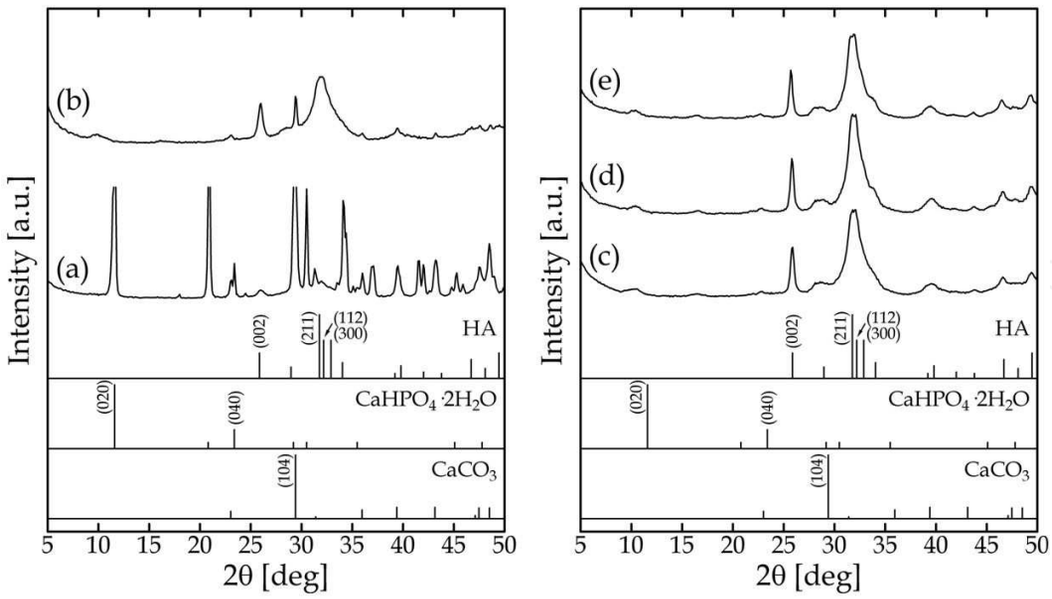

Figure 10. XRD pattern of 1 h-milled samples (a) before heating and after heating at 80°C for (b) 30 min, (c) 1 h, (d) 3 h, and (e) 5 h.

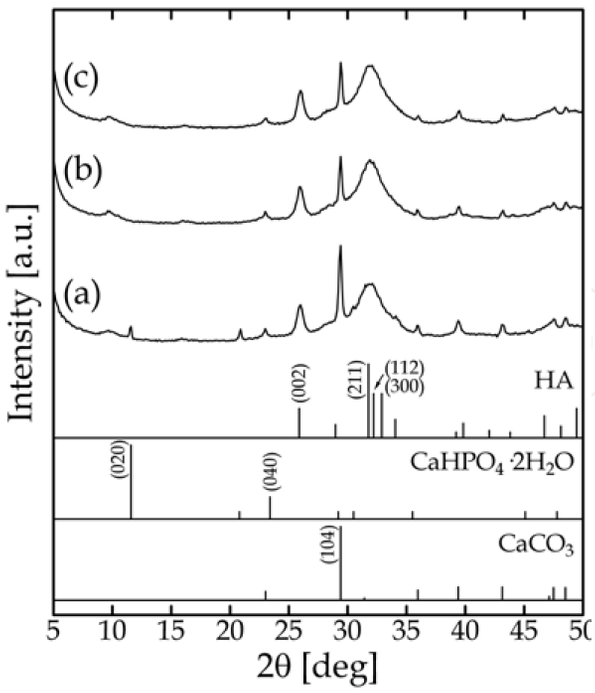

Figure 11. XRD pattern of 3 h-milled samples (a) before heating and after heating at 40°C for (b) 1 h, and (c) 5 h.

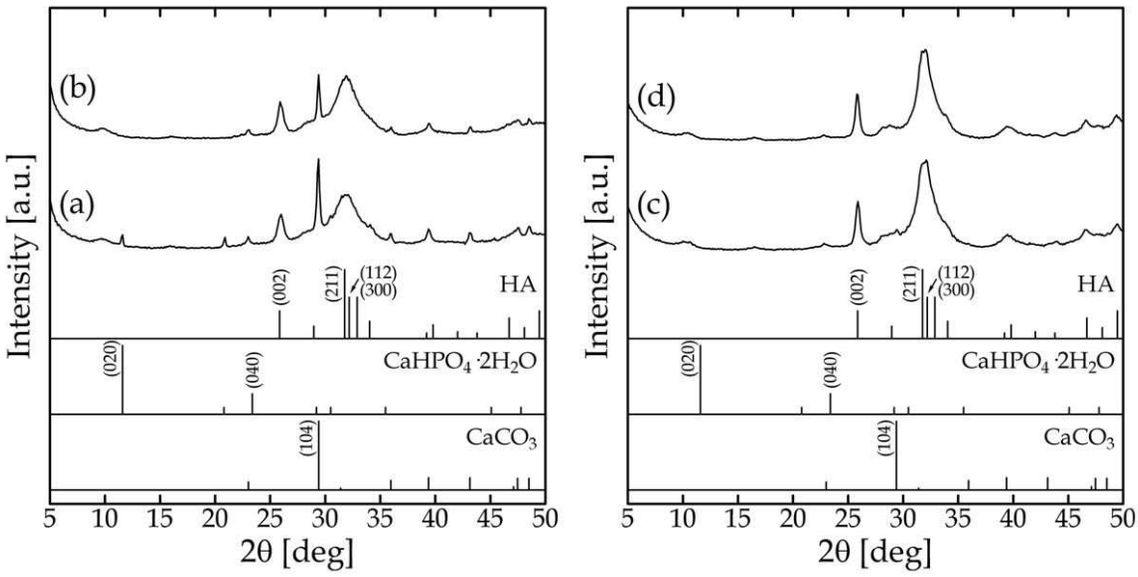

Figure 12. XRD pattern of 3 h-milled samples (a) before heating and after heating at 60°C for (b) 1 h, (c) 3 h, and (d) 5 h.

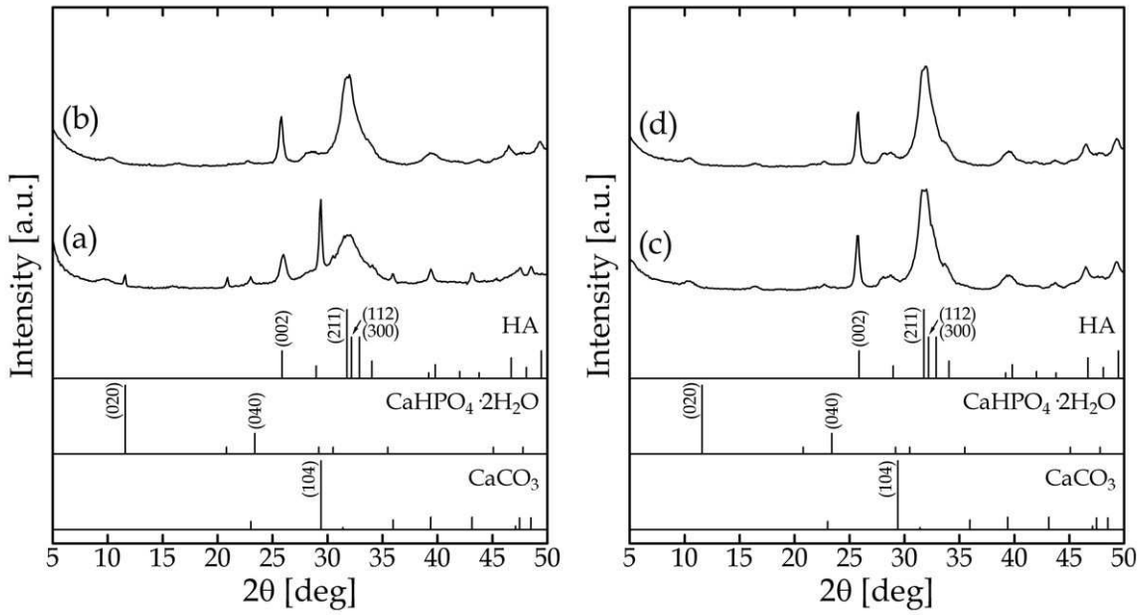

Figure 13. XRD pattern of 3 h-milled samples (a) before heating and after heating at 80°C for (b) 1 h, (c) 3 h, and (d) 5 h.

http://dx.doi.org/10.5772/54344

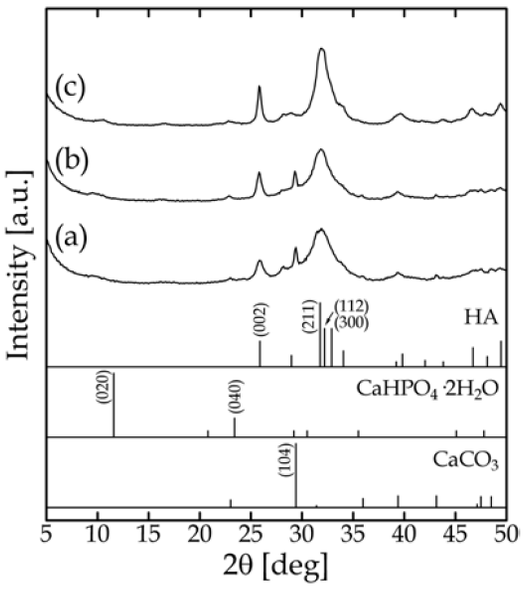

Figure 14. XRD pattern of 12 h-milled samples (a) before heating and after heating at 80°C for (b) 30 min, and (c) 1 h.

3. Synthesis and hyperthermia property of magnetite/hydroxyapatite nanocomposites

In the synthesis of Fe_3O_4/HA nanocomposites, first a suspension of superparamagnetic Fe_3O_4 nanoparticles was prepared according to a mechanochemical method reported in elsewhere [11]. This method provides Fe_3O_4 from ferric hydroxide (goethite) in the absence of a reducing agent; goethite is reduced to ferrous hydroxide by mechanochemical effects and the solid phase reaction between ferrous hydroxide and goethite generates Fe_3O_4 [16]. Subsequently, HA nanoparticles were synthesized in the suspension of Fe_3O_4 nanoparticles in the same container by the mechanochemical method mentioned above.

4.5 mmol of ferric chloride hexahydrate ($FeCl_3$ $6H_2O$) was dissolved in 60 ml of deionized and deoxygenated water. To precipitate amorphous ferric hydroxides (mostly, goethite), a proper amount of 1.0 M sodium hydroxide (NaOH) solution was dropped into the solution which was magnetically stirred under a continuous flow of argon at room temperature. The pH was adjusted to higher than 13. A brown suspension thus prepared was placed in a gas-tight milling pot (inner diameter 90 mm, capacity 500 ml) made of 18%Cr–8%Ni stainless steel. Stainless steel balls (diameter 3.2 mm) were used as the milling media. The charged volume including the voids among the balls was about 40% of the pot capacity. The pot was purged of air, filled with argon, and sealed. The milling was performed at room temperature for 11 h. The rotational speed was 140 rpm, corresponding to the ideal critical rotational speed.

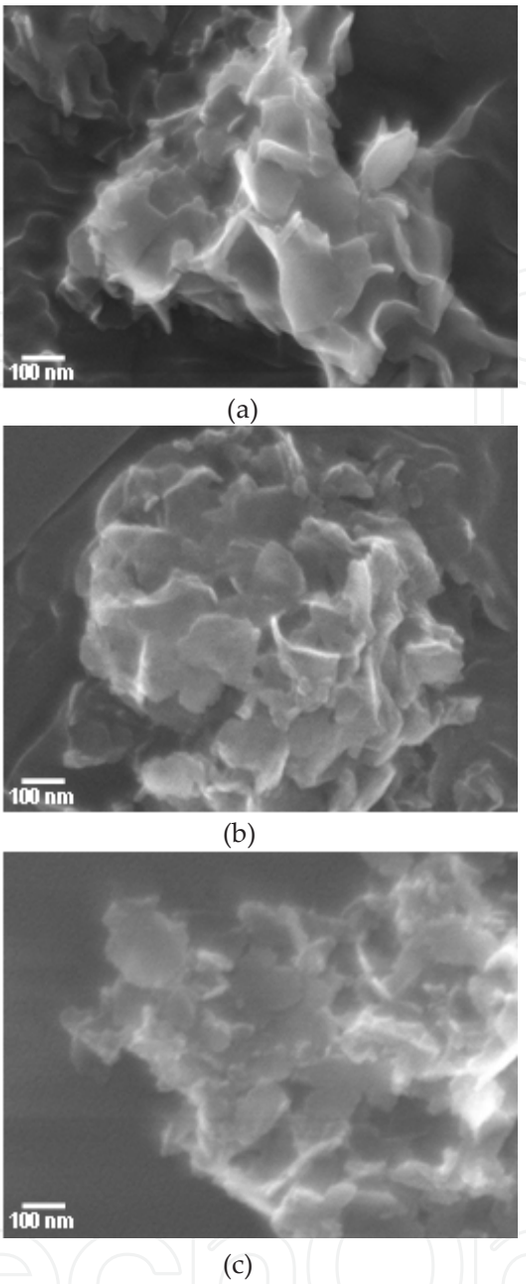

Figure 15. SEM image of samples obtained by milling for (a) 1 h, (b) 3 h, and (c) 12 h, followed by heating at 80°C for 1 h.

The XRD pattern of Fe_3O_4 nanoparticles thus prepared is shown in Figure 16. The Fe_3O_4 nanoparticles had a high crystallinity and an average crystallite size of 11.7 nm which was calculated from the full width at half-maximum (FWHM) of the Fe_3O_4 (311) diffraction peak at 2θ=35.5° using Scherrer's formula. The lattice constant was determined to be 8.387 Å from several diffraction angles showing high intensity peaks, which was close to the standard value of Fe_3O_4 (8.396 Å) as compared to that of maghemite (8.345 Å). Figure 16 also shows that no reflections indicating formation of other compounds were observed. This indicates the Fe_3O_4 nanoparticles were high purity.

http://dx.doi.org/10.5772/54344

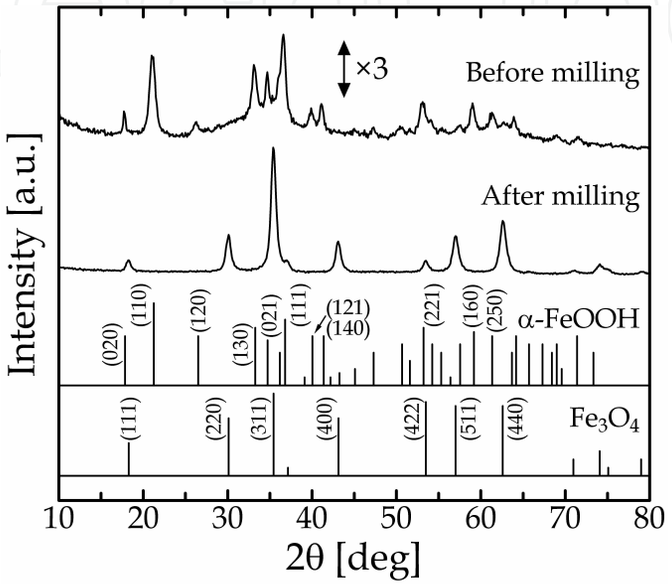

Figure 16. XRD pattern of Fe_3O_4 nanoparticles prepared by mechanochemical method.

As shown in Figure 17, the SEM image indicated that the Fe_3O_4 nanoparticles had a diameter of approximately 10–20 nm, which almost agreed with the average crystallite size (11.7 nm). The hydrodynamic size (number basis) was measured by dynamic light scattering (DLS; Zetasizer Nano ZS, Malvern Instruments) for a dispersion, as shown in Figure 18. The median diameter was determined to be 16.4 nm from the size distribution, which was also near the average crystallite size. These results reveal that the Fe_3O_4 nanoparticles have a single-crystal structure.

The magnetic property (magnetization-magnetic field hysteretic cycle) was analyzed using a superconducting quantum interference device (SQUID) magnetometer (Quantum Design model MPMS) at room temperature in the rage of magnetic field between –10 kOe and 10 kOe. Figure 19 shows the magnetization-magnetic field curve. The Fe_3O_4 nanoparticles had a low coercivity (4 Oe), showing superparamagnetism. The saturation magnetization (78 emu/g) was a little lower than that of the corresponding bulk (=92 emu/g) because of the smaller size [17].

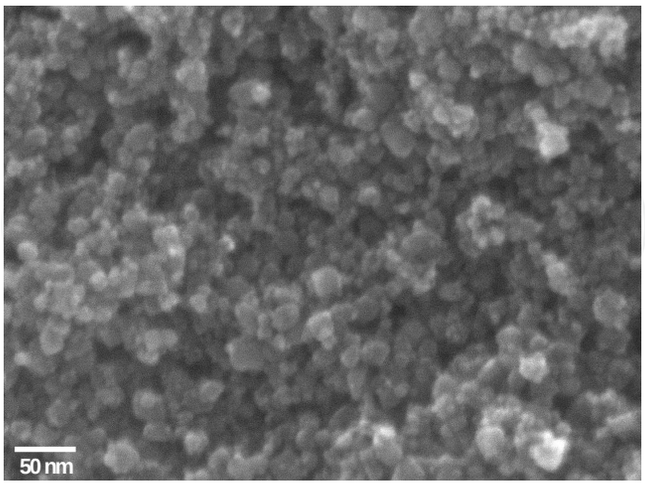

Figure 17. SEM image of Fe_3O_4 nanoparticles prepared by mechanochemical method.

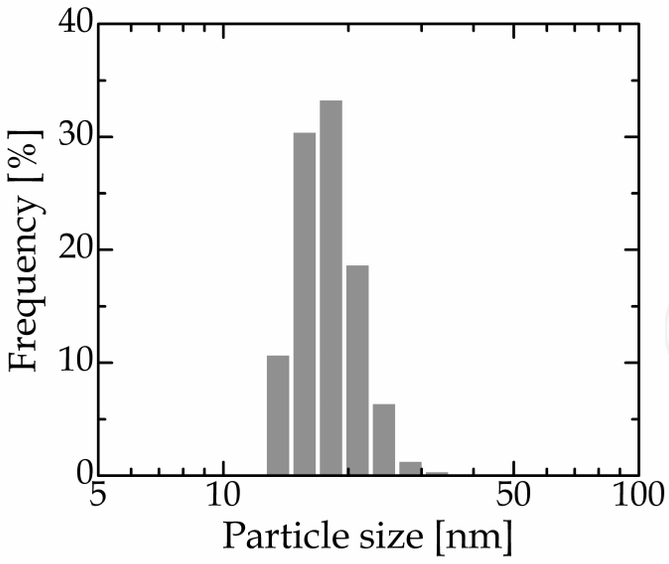

Figure 18. DLS particle size distribution of Fe_3O_4 nanoparticles prepared by mechanochemical method.

http://dx.doi.org/10.5772/54344

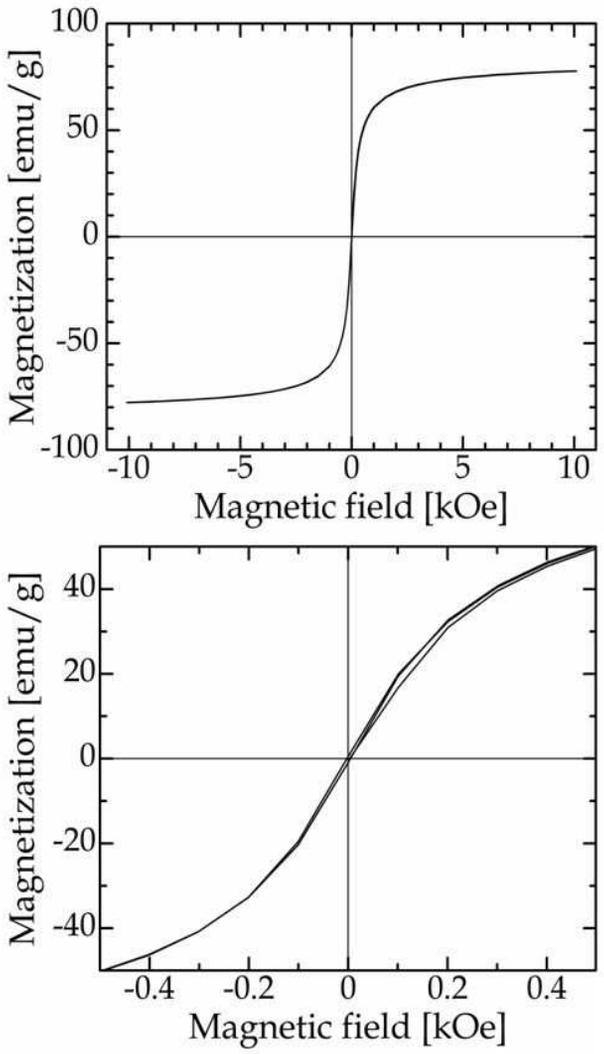

Figure 19. Magnetization-magnetic field curve of Fe_3O_4 nanoparticles prepared by mechanochemical method.

After the suspension of Fe_3O_4 nanoparticles was prepared, the milling pot was opened, and then predetermined amounts of $CaHPO_4$ $2H_2O$ and $CaCO_3$ were added to the suspension. Their amounts were adjusted so that the mass concentration of Fe_3O_4 nanoparticles in the Fe_3O_4/HA nanocomposite was 10, 20, and 30 mass%. In order to prevent the oxidation of Fe_3O_4 during milling, the pot was purged of air, filled with argon, and sealed prior to milling. The suspension was milled at a rotational speed of 140 rpm for 1 h at room temperature, followed by the heating at 80°C for 1 h.

Figure 20 shows the XRD pattern of Fe_3O_4/HA nanocomposites with different Fe_3O_4 concentrations. It was confirmed that the nanocomposites consisted of Fe_3O_4 and HA having no by-products regardless of the Fe_3O_4 concentration. The average crystallite sizes of Fe_3O_4 and HA were calculated from the FWHM of the Fe_3O_4 (311) plane at 2θ=35.5° and the HA (002) plane at 2θ=25.9°, respectively, using Scherrer's formula, and listed in Table 1. The average crystallite sizes of Fe_3O_4 and HA were almost constant regardless of the concentration of Fe_3O_4 in the Fe_3O_4/HA nanocomposites.

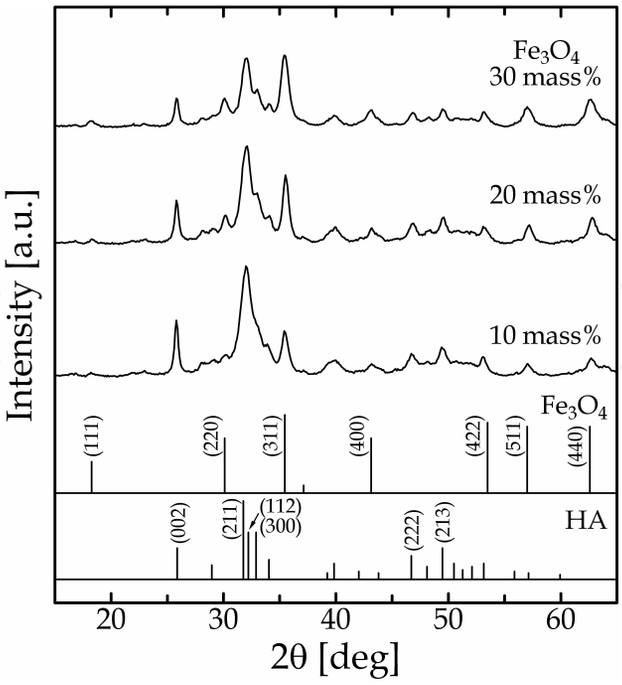

Figure 20. XRD pattern of Fe_3O_4/HA nanocomposites with different Fe_3O_4 concentrations.

Fe_3O_4 concentration	Crystallite size of Fe_3O_4	Crystallite size of HA
10 mass%	11.3 nm	20.3 nm
20 mass%	12.8 nm	18.8 nm
30 mass%	9.8 nm	17.8 nm

Table 1. Crystallite sizes of Fe_3O_4 and HA in Fe_3O_4/HA nanocomposites.

Figure 21 shows the SEM image of nanocomposite containing 30 mass% Fe_3O_4 as an example. The Fe_3O_4 nanoparticles with a diameter of about 20 nm were distributed homogeneously in the HA matrix without forming large aggregates. It was confirmed that nanometer-sized Fe_3O_4/HA composite particles were successfully synthesized.

The magnetic hyperthermia property was evaluated using an apparatus reported in elsewhere [18]. A proper amount of Fe_3O_4/HA nanocomposite powder sample was placed in a polystyrene tube with a diameter of 16 mm, and packed by tapping the tube. The packing volume was constant at 0.8 cm^3 regardless of the Fe_3O_4 concentration. The temperature increase was measured in an AC-magnetic field using an optical fiber thermometer. The frequency and amplitude of the AC-magnetic field were 600 kHz and 2.9 kA/m, respectively. Figure 22 shows the temperature increase for the nanocomposites in the AC-magnetic field. As the Fe_3O_4 concentration increased, the temperature increased more rapidly. When the Fe_3O_4 concentration was 30 mass%, the temperature increase of 40°C was achieved only after

http://dx.doi.org/10.5772/54344

about 20 sec. This result supports that the Fe_3O_4/HA nanocomposites synthesized by this mechanochemical process exhibit a good hyperthermia property [1–4].

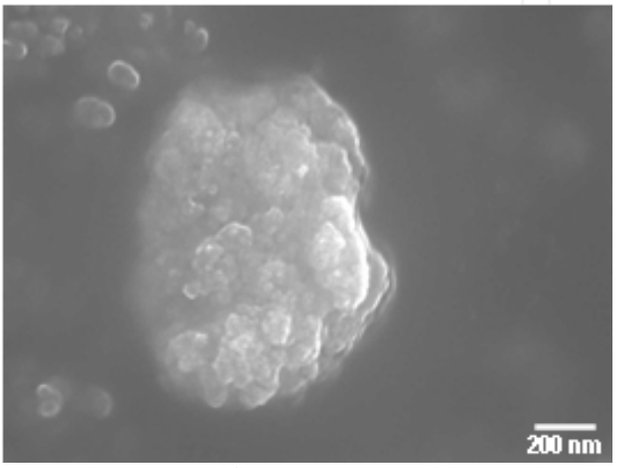

Low-magnification observation

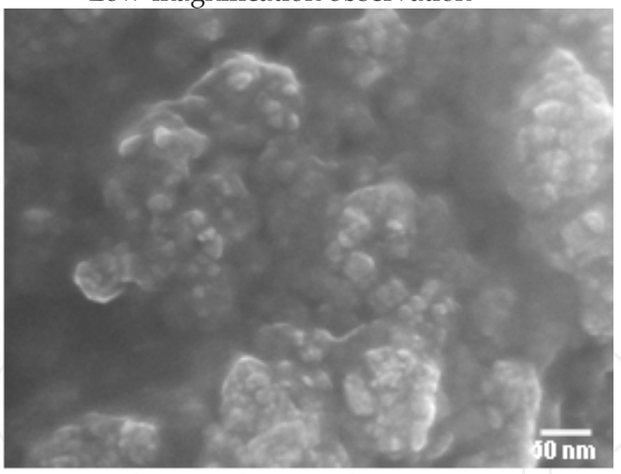

High-magnification observation

Figure 21. SEM images of 30 mass% Fe_3O_4/HA nanocomposites.

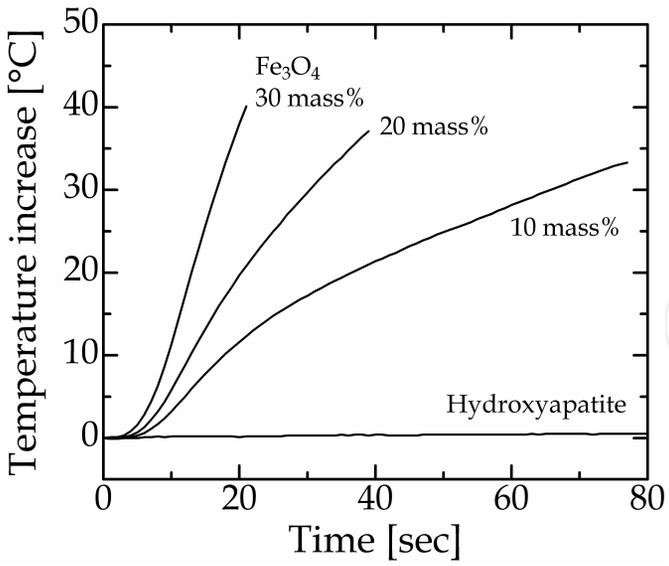

Figure 22. Temperature profiles of HA nanoparticles and Fe_3O_4/HA nanocomposites with different Fe_3O_4 concentrations in AC-magnetic field.

4. Conclusion

A mechanochemical method for the simple synthesis of Fe_3O_4/HA nanocomposites has been developed, in which superparamagnetic Fe_3O_4 nanoparticles and HA nanoparticles are sequentially prepared in a single horizontal tumbling ball mill at room temperature under wet conditions. First, the synthesis process of HA (containing no Fe_3O_4) was optimized. The obtained HA samples were characterized by XRD, DSC, and SEM. The influence of conditions on the formation of HA nanoparticles was investigated. Mechanochemical effects induced during wet milling promoted the reactions between $CaHPO_4$ $2H_2O$ and $CaCO_3$ forming HA even at room temperature. The combination of milling and heating (aging) of the suspension of $CaHPO_4$ $2H_2O$ and $CaCO_3$ can produce efficiently HA for short periods of time. The optimum operating conditions in the synthesis of HA were determined as follows: a rotational speed of 140 rpm, a milling time of 1 h, an aging temperature of 80°C, and an aging time of 1 h. Next, the synthesis of Fe_3O_4/HA nanocomposites was investigated. The mechanochemically synthesized Fe_3O_4 nanoparticles, of which the median diameter was 16 nm, had a high crystallinity and a high saturation magnetization of 78 emu/g, and showed superparamagnetism. The wet mechanochemical process also contributed to the distribution of Fe_3O_4 nanoparticles in the HA matrix. The Fe_3O_4/HA nanocomposites were confirmed to have a good hyperthermia property through the measurement of temperature increase in an AC-magnetic field. For example, the 30 mass% Fe_3O_4/HA nanocomposites showed the temperature increase of 40°C after about 20 sec under a frequency of 600 kHz and an amplitude of 2.9 kA/m. Consequently, the Fe_3O_4/HA nanocomposites thus synthesized were found to be a promising material for hyperthermia therapy.

http://dx.doi.org/10.5772/54344

Acknowledgements

The author would like to thank Professor Kenya Murase of Osaka University for his support in measuring temperature profile of nanocomposites.

Author details

Tomohiro Iwasaki*

Department of Chemical Engineering, Osaka Prefecture University, Japan

References

[1] Murakami S, Hosono T, Jeyadevan B, Kamitakahara M, Ioku K. Hydrothermal synthesis of magnetite/hydroxyapatite composite material for hyperthermia therapy for bone cancer. Journal of the Ceramic Society of Japan 2008;116(9) 950–954.

[2] Andronescu E, Ficai M, Voicu G, Ficai D, Maganu M, Ficai A. Synthesis and characterization of collagen/hydroxyapatite: magnetite composite material for bone cancer treatment. Journal of Materials Science: Materials in Medicine 2010;21(7) 2237–2242.

[3] Inukai A, Sakamoto N, Aono H, Sakurai O, Shinozaki K, Suzuki H, Wakiya N. Synthesis and hyperthermia property of hydroxyapatite-ferrite hybrid particles by ultrasonic spray pyrolysis. Journal of Magnetism and Magnetic Materials 2011;323(7) 965–969.

[4] Tampieri A, D'Alessandro T, Sandri M, Sprio S, Landi E, Bertinetti L, Panseri S, Pepponi G, Goettlicher J, Bañobre-López M, Rivas J. Intrinsic magnetism and hyperthermia in bioactive Fe-doped hydroxyapatite. Acta Biomaterialia 2012;8(2) 843–851.

[5] Dong L, Zhu Z, Qiu Y, Zhao J. Removal of lead from aqueous solution by hydroxyapatite/magnetite composite adsorbent. Chemical Engineering Journal 2010;165(3) 827–834.

[6] Wang X. Preparation of magnetic hydroxyapatite and their use as recyclable adsorbent for phenol in wastewater. Clean—Soil, Air, Water 2011;39(1) 13–20.

[7] Xie H, Li X, Cheng C, Wu D, Zhang S, Jiao Z, Lan Y. Kinetic and thermodynamic sorption study of radiocobalt by magnetic hydroxyapatite nanoparticles. Journal of Radioanalytical and Nuclear Chemistry 2012;291(2) 637–647.

[8] Yang Z, Gong X, Zhang C. Recyclable Fe_3O_4/hydroxyapatite composite nanoparticles for photocatalytic applications. Chemical Engineering Journal 2010;165(1) 117–121.

[9] Liu Y, Zhong H, Li L, Zhang C. Temperature dependence of magnetic property and photocatalytic activity of Fe_3O_4/hydroxyapatite nanoparticles. Materials Research Bulletin 2010;45(12) 2036–2039.

[10] Covaliu CI, Georgescu G, Jitaru I, Neamtu J, Malaeru T, Oprea O, Patroi E. Synthesis and characterization of a hydroxyapatite coated magnetite for potential cancer treatment. Revista de Chimie 2009;60(12) 1254–1257.

[11] Iwasaki T, Sato N, Kosaka K, Watano S, Yanagida T, Kawai T. Direct transformation from goethite to magnetite nanoparticles by mechanochemical reduction. Journal of Alloys and Compounds 2011;509(4) L34–L37.

[12] Silva CC, Pinheiro AG, Miranda MAR, Góes JC, Sombra ASB. Structural properties of hydroxyapatite obtained by mechanosynthesis. Solid State Sciences 2003;5(4) 553–558.

[13] Shu C, Yanwei W, Hong L, Zhengzheng P, Kangde Y. Synthesis of carbonated hydroxyapatite nanofibers by mechanochemical methods. Ceramics International 2005;31(1) 135–138.

[14] Wu SC, Hsu HC, Wu YN, Ho WF. Hydroxyapatite synthesized from oyster shell powders by ball milling and heat treatment. Materials Characterization 2011;62(12) 1180–1187.

[15] Iwasaki T, Yabuuchi T, Nakagawa H, Watano S. Scale-up methodology for tumbling ball mill based on impact energy of grinding balls using discrete element analysis. Advanced Powder Technology 2010;21(6) 623–629.

[16] Iwasaki T, Sato N, Nakamura H, Watano S. Aqueous-phase synthesis of crystalline magnetite nanoparticles by a new mechanochemical method. In: proceedings of the 5th Asian Particle Technology Symposium, APT2012, 2–5 July 2012, Singapore.

[17] Lee J, Isobe T, Senna M. Magnetic properties of ultrafine magnetite particles and their slurries prepared via in-situ precipitation. Colloids and Surfaces A: Physicochemical and Engineering Aspects 1996;109, 121–127.

[18] Murase K, Oonoki J, Takata H, Song R, Angraini A, Ausanai P, Matsushita T. Simulation and experimental studies on magnetic hyperthermia with use of superparamagnetic iron oxide nanoparticles. Radiological Physics and Technology 2011;4(2) 194–202.